# Neutron polarization analysis study of the frustrated magnetic ground state of $\beta$-$Mn_{1-x}Al_x$

J. R. Stewart* and K. H. Andersen
*Institut Laue-Langevin, 6 rue Jules Horowitz, F-38042 Grenoble, France*

R. Cywinski
*Department of Physics and Astronomy, University of Leeds, Leeds, LS2 9JT, United Kingdom*
(Received 15 May 2008; revised manuscript received 30 June 2008; published 28 July 2008)

We have performed a neutron polarization analysis study of the short-range nuclear and magnetic correlations present in the dilute alloy, $\beta$-$Mn_{1-x}Al_x$ with $0.03 \leq x \leq 0.16$, in order to study the evolution of the magnetic ground state of this system as it achieves static spin-glass order at concentrations $x > 0.09$. To this end we have developed a reverse–Monte Carlo algorithm which has enabled us to extract Warren-Cowley nuclear short-range order parameters and magnetic spin correlations. Using conventional neutron powder diffraction, we show that the nonmagnetic Al substituents preferentially occupy the magnetic site II Wyckoff positions in the $\beta$-Mn structure—resulting in a reduction of the magnetic topological frustration of the Mn atoms. These Al impurities are found to display strong anticlustering behavior. The magnetic spin correlations are predominantly antiferromagnetic, persisting over a short range which is similar for all the samples studied—above and below the spin-liquid-spin-glass boundary—while the observed static (disordered) moment is shown to increase with increasing Al concentration.

DOI: 10.1103/PhysRevB.78.014428 PACS number(s): 61.43.Bn, 75.10.Nr

## I. INTRODUCTION

The mechanisms of magnetic moment formation and localization in transition metals and the magnetic spin configurations of geometrically frustrated magnets are two of the most interesting problems in modern magnetism. According to the self-consistent renormalization (SCR) theory of Moriya[1] the characterization of the magnetic properties of transition metal magnets, from a purely itinerant electron model to a localized moment model, depends only on the properties of the spin fluctuations in the system. According to Moriya's theory, by varying parameters such as magnetic field, external pressure and chemical pressure, nearly and weakly magnetic 3*d* metals follow a smooth evolution from an itinerant electron system with delocalized, small amplitude longitudinal spin fluctuations to a state in which the magnetic moments appear to be more localized with saturated transverse spin fluctuations.[2] A good example of such a system is $\beta$-Mn(Al).

Pure $\beta$-Mn is the only stable allotrope of elemental manganese not to display any magnetic order down to the lowest temperatures studied. However, over the last 30 years, a wealth of evidence has accumulated which suggests that $\beta$-Mn metal is on the verge of magnetic order and moment localization. $\beta$-Mn displays a complicated nuclear structure with the simple cubic $P4_132$ space group. Each unit cell contains eight Mn atoms at Wyckoff position 8*c* (site I) and twelve Mn atoms at position 12*d* (site II).[3] A depiction of the $\beta$-Mn lattice with the site I and site II sublattices is shown in Fig. 1. Nuclear magnetic relaxation measurements by Kohori and co-workers[5] have shown that the nuclear spin-lattice relaxation rate $1/T_1$ for the site II Mn nuclei displays a $\sqrt{T}$ temperature dependence characteristic of a nearly antiferromagnetic (AF) metal according to SCR theory. In contrast, for the site I Mn atoms they find a spin-lattice relaxation rate which is around a factor of 20 times lower than that of site II, suggesting that itinerant magnetic moment formation occurs predominantly on site II. In addition, the observation of a strongly enhanced electronic coefficient of the specific heat,[6] $\gamma$, has led to the conjecture that the magnetic ground state of $\beta$-Mn is dominated by fast zero-point spin fluctuations, which inhibit the formation of a long-range ordered magnetic structure at low temperatures. This picture was confirmed by our investigation of the temperature dependence of the spin dynamics of $\beta$-Mn using time-of-flight inelastic neutron scattering.[7] In this study, it was found that the spin dynamics of $\beta$-Mn could be described by an extremely wide (top-hat) distribution of spin-relaxation energies between 0 and 40 meV at low temperatures, this broad distribution being indicative of non-Fermi-liquid (NFL) spin relaxation.[8] This conjecture was confirmed by an analysis of the electrical resistivity which was found to follow a $T^{3/2}$ temperature dependence.[7] This, again, corresponds to the predicted temperature dependence of the resistivity for a metal on the verge of antiferromagnetic order (i.e., a $T_N=0$ antiferromagnet) according to SCR theory.

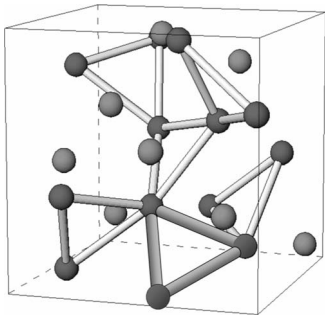

FIG. 1. The $P4_132$ simple cubic crystal structure of $\beta$-Mn, with the site I Mn atoms in light gray and the site II Mn atoms in dark gray. The "distorted windmill" of corner-sharing triangles perpendicular to local ⟨111⟩ axes is depicted (Refs. 3 and 4).

 

It has long been known that the substitution of dilute quantities of transition metal impurities, as well as nontransition metals such as Al, In and Sn, leads to the rapid reduction of $\gamma$, and hence damping of the broad spin fluctuations leading to a static magnetic ground state.[9] This ground state was originally interpreted—mostly on the basis of indirect methods such as NMR and Mössbauer—as being long-range antiferromagnetic. Neutron-diffraction measurements,[10–12] however, have until recently, failed to observe long-range magnetic order in any $\beta$-Mn alloy. Long-range order has, in fact, recently been discovered in alloys of $\beta$-Mn with Os and Ru using neutron powder diffraction.[13–15] All other $\beta$-Mn alloys studied to date show no signs of long-range magnetic order, even though they commonly display properties indicative of a static ground state.

This issue was first addressed by the group of Shiga and co-workers[10,16] who pointed out the possibility of topological frustration of antiferromagnetically correlated moments in the $\beta$-Mn site II sublattice. They drew on the previous work of Shoemaker *et al.*[3] who described the site II sublattice as a distorted network of corner-sharing triangles—termed a "distorted windmill," with the plane of each triangle being normal to each of the local $\langle 111 \rangle$ axes, and each site II Mn atom shared between three triangles (see Fig. 1).

This "distorted windmill" structure was later confirmed to be frustrated,[17] assuming simple mean-field Heisenberg near-neighbor exchange between the site II Mn moments and a *perfect* $\beta$-Mn lattice; i.e., one in which the triangles of site II Mn atoms are equilateral. Intriguingly, however, the Mn spin degrees of freedom are only "fully frustrated" along the $\langle 111 \rangle$ directions, i.e., normal to the plane of the triangles. Here the phrase "fully frustrated" refers to the fact that the ground-state energy eigenvalues of the Heisenberg exchange matrix are completely dispersionless—i.e., infinitely degenerate. In other directions in reciprocal space, the ground-state energy eigenvalues are found not to be degenerate. Thus the $\beta$-Mn lattice is somewhat less frustrated than the so-called *fully frustrated lattices* (FFL), namely, the pyrochlore and kagomé lattices, in which the ground-state energy eigenvalues are degenerate over the entire Brillouin zone. It should be noted here that if higher order (next-nearest-neighbor) interactions are taken into account, then either $q=0$ or incommensurate magnetic long-range order is predicted using this model.[17]

In this study we will examine the nature of the static magnetic ground state of $\beta$-Mn(Al). Al is substitutable in $\beta$-Mn up to around the 22 at.% level. This substitution results in a volume expansion of the $\beta$-Mn lattice, which is roughly linear, at a rate of approximately 0.15% per at.% Al.[16,18] NMR and neutron-scattering studies[16] show that the substitution of Al for Mn results in a slowing down of the spin dynamics compared to pure $\beta$-Mn—concomitant with a strong reduction in the electronic specific-heat coefficient, $\gamma$. Our own muon spin-relaxation ($\mu$SR) studies[19] enabled us to construct a magnetic phase diagram of the $\beta$-$Mn_{1-x}Al_x$ system, indicating transitions from the paramagnetic phase to a static spin-glass-like phase at low temperatures. This phase diagram derived from our muon studies is shown in Fig. 2. There are two distinct regions of the $\beta$-$Mn_{1-x}Al_x$ phase diagram. For Al concentrations $<9$ at. % the transitions to a static magnetic ground state (albeit with evidence of significant residual spin dynamics below this transition) occur at temperatures $T_g \leq 6$ K, with simple exponential spin relaxation being observed in the paramagnetic regime above the transition. For Al concentrations $>9$ at. %, $T_g \geq 24$ K, and the paramagnetic spin dynamics display stretched exponential relaxation indicative of a spin glass.[20] This crossover in the magnetic phase diagram of $\beta$-$Mn_{1-x}Al_x$, termed the spin-liquid to spin-glass transition, appears to be rather abrupt. Similar crossover behavior was observed in NMR studies by Nakamura and co-workers.[16]

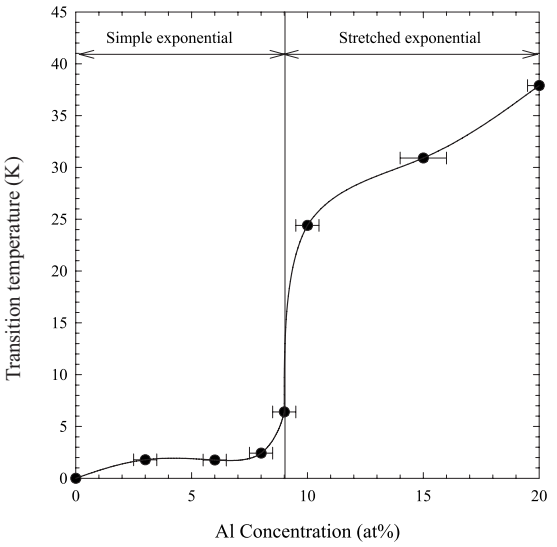


FIG. 2. The magnetic phase diagram of $\beta$-$Mn_{1-x}Al_x$ as inferred from $\mu$SR measurements of the spin dynamics (Ref. 19). The diagram is split into two regions; for $\leq 9$ at. % Al, the relaxation was found to be simple exponential in nature and the transitions are at very low temperature. For $>9$ at. % Al, the relaxation followed a stretched exponential form, and the transition temperatures were greatly enhanced.

In our present study, we will attempt to elucidate the configurational nature of the $\beta$-$Mn_{1-x}Al_x$ magnetic ground state for Al concentrations above and below the spin-liquid to spin-glass transition concentration of $x=0.09$. We have carried out this study using both conventional neutron powder-diffraction and neutron polarization analysis of the diffuse neutron scattering. Analysis of the conventional neutron powder-diffraction patterns permits the characterization of the spatially averaged nuclear structure, and allows the determination of the site-substitutional properties of the Al impurity atoms in the $\beta$-Mn lattice. Analysis of the diffuse neutron scattering enables the analysis of any deviations of the nuclear structure from perfect order, such as clustering of the Al impurity atoms. Since long-range magnetic order is not achieved in $\beta$-$Mn_{1-x}Al_x$ alloys, any spin-configurational short-range order will also show up in the diffuse scattering cross section. The technique of neutron polarization analysis enables the separation of nuclear and magnetic contributions to the total scattering, allowing full, unambiguous and simultaneous determination of any nuclear and magnetic short-range order present in the system.

## II. SAMPLE PREPARATION AND CHARACTERIZATION

All of the $\beta$-$Mn_{1-x}Al_x$ samples used in this study were prepared by the arc-melting technique in which high-purity constituent metals are melted together using an electric arc in a low-pressure pure argon atmosphere. After melting, the $\beta$-Mn phase was stabilized by annealing the melted ingots under a low argon pressure in sealed quartz containers at 900° C for 24 h. The $\beta$-Mn phase was retained at room temperature by rapid quenching of the ingots in water. Preliminary structural analysis of the samples and verification of the $\beta$ phase of Mn (and more importantly, the absence of the antiferromagnetic $\alpha$-Mn phase) were achieved using x-ray diffraction. Magnetization measurements of each of the samples using an Oxford Instruments vibrating sample magnetometer (VSM) showed the same features as previously reported by us[19] and by Nakamura and co-workers[16]—i.e., an almost temperature independent magnetization for low Al concentrations, moving over to a spin-glass-like response for higher Al concentrations with a characteristic bifurcation of the zero-field cooled and field cooled magnetization branches.

## III. NEUTRON POWDER-DIFFRACTION MEASUREMENTS

In order to determine the structural properties of $\beta$-$Mn_{1-x}Al_x$ as a function of Al concentration $x$, we have performed conventional neutron powder-diffraction measurements of six $\beta$-$Mn_{1-x}Al_x$ samples with $x=0$, 0.03, 0.06, 0.08, 0.1 and 0.2, using the time-of-flight diffractometer LAD at the ISIS spallation neutron source, in the U.K.

The measured coherent elastic neutron-scattering intensity is given by

$$I \propto \frac{d\sigma}{d\Omega} = \frac{(2\pi)^3}{V} \sum_{h,k,l} \delta(\vec{Q} - \vec{G}_{hkl}) |F(\vec{G}_{hkl})|^2, \qquad (1)$$

where $\vec{Q}$ is the neutron wave-vector transfer (i.e., the difference between the incoming and outgoing neutron wave vectors), $\vec{G}_{hkl}$ is the reciprocal lattice vector for the (h k l) crystal plane and $F(\vec{G}_{hkl})$ is the structure factor defined by

$$|F(\vec{G}_{hkl})|^2 = \left| \sum_i b_i \exp(i\vec{G}_{hkl} \cdot \vec{R}_i) \right|^2, \qquad (2)$$

where $\vec{R}_i$ is the position vector and $b_i$ is the neutron-scattering length of the $i^{\text{th}}$ atom in the unit cell. From Eq. (2) we note that the intensity of a particular Bragg peak will depend on the average neutron-scattering length $\bar{b} = \frac{1}{N}\Sigma_{i=1,N} b_i$ for a particular crystal plane. The intensity of the Bragg peaks therefore provides information on the position of the Al substituent atoms on the host $\beta$-Mn matrix. In the case of $\beta$-$Mn_{1-x}Al_x$ the situation is particularly favorable since the individual scattering lengths of Mn and Al are roughly equal in magnitude, but of opposite sign ($b_{Mn} = -3.73 \times 10^{-15}$ m and $b_{Al} = +3.45 \times 10^{-15}$ m). This results in a strong variation in the Bragg intensities as a function of Al concentration and crystallographic position. Any site-substitutional preferences of the Al impurity atoms are then readily determined by neutron powder diffraction.

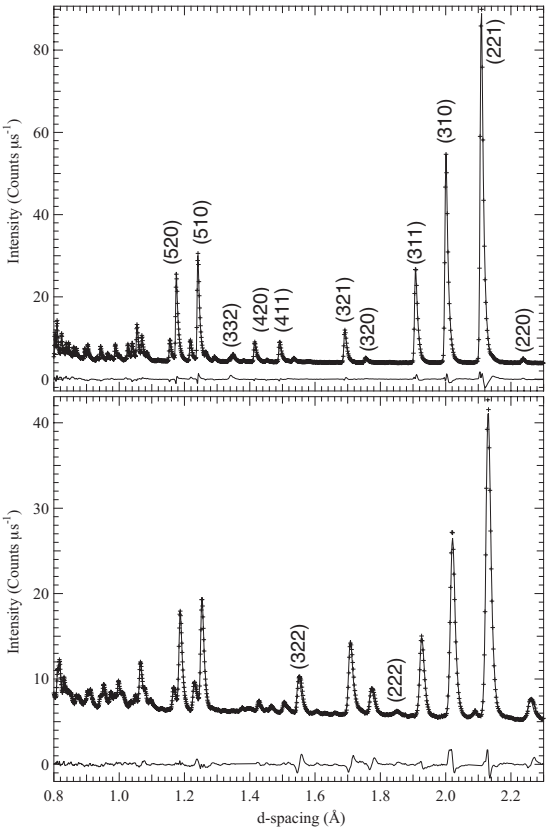


FIG. 3. Neutron powder-diffraction patterns of $\beta$-$Mn_{1-x}Al_x$ with $x=0$ (top) and $x=0.2$ (bottom). The solid line is a model fit to the data, determined from Rietveld refinement. The difference curve between model and data is also shown.

The neutron powder-diffraction patterns of $\beta$-$Mn_{1-x}Al_x$ with $x=0$ and $x=0.2$ are shown in Fig. 3. Several Bragg reflections are marked, showing clearly the effect of Al substitution on the relative peak intensities. The diffraction patterns were analyzed using the Rietveld refinement program GSAS.[21] The modeled diffraction patterns are shown as solid lines in Fig. 3 together with the difference curve between model and data.

For all $\beta$-$Mn_{1-x}Al_x$ samples studied, it was found that the Al atoms strongly preferred the site II 12*d* crystallographic site. The modeling of the data therefore was performed with Al substituents solely occupying the site II $\beta$-Mn sublattice. This enabled us to extract the actual Al concentration for each sample. The refined fitting parameters obtained from the Rietveld refinements of the data for all samples studied are presented in Table I. The Al impurity concentration dependence of the $\beta$-Mn unit-cell volume extracted from the lattice constants in Table I is shown in Fig. 4. This shows a clear linear increase in the unit-cell volume at a rate of $0.17 \pm 0.01\%$ per at. % Al, in agreement with the value found by Nakamura and co-workers.[16]

## IV. NEUTRON POLARIZATION ANALYSIS STUDIES

In order to examine the nuclear and magnetic short-range order present in the $\beta$-$Mn_{1-x}Al_x$ alloys under investigation

TABLE I. Fitting parameters obtained by Rietveld refinement of the neutron powder-diffraction pattern of $\beta$-$Mn_{1-x}Al_x$. $x_{nom}$ and $x_{calc}$ are the nominal and calculated Al concentrations, $a$ is the cubic lattice constant, $d_I$ and $d_{II}$ are the site I and site II near-neighbor distances and $R_{wp}$ is the weighted Bragg $R$-factor from the GSAS Rietveld refinement.

| $x_{nom}$ | $a$ (Å) | $d_I$ (Å) | $d_{II}$ (Å) | $x_{calc}$ | $R_{wp}$ |
|---|---|---|---|---|---|
| 0 | 6.320 | 2.367 | 2.646 | 0 | 3.95 |
| 0.03 | 6.329 | 2.368 | 2.653 | 0.029 | 2.91 |
| 0.06 | 6.335 | 2.368 | 2.654 | 0.036 | 4.19 |
| 0.08 | 6.341 | 2.369 | 2.658 | 0.058 | 3.20 |
| 0.1 | 6.350 | 2.370 | 2.663 | 0.073 | 4.07 |
| 0.2 | 6.379 | 2.377 | 2.682 | 0.163 | 3.10 |

we have performed a neutron polarization analysis study of the diffuse scattering present in these alloys. Specifically, we have used the technique of "*xyz*" neutron polarization analysis (*xyz*-NPA) developed by Schärpf,[22] which allows analysis of the neutron polarization on a wide angle multidetector-type neutron spectrometer. This technique is most especially useful for diffuse scattering studies of disordered materials. The diffuse neutron-scattering contribution—i.e., that portion of the scattering found between the Bragg reflections—can have many causes, examples of which include the following: the presence of nuclear isotopes, nuclear spin-incoherent scattering, random or nonrandom solid solution materials (e.g., binary alloys), interstitial defects, vacancies and internal strain. If the material under investigation is magnetic, or contains some magnetic species, then any disordered (paramagnetic) moment will result in diffuse scattering. Long-range ordered magnetic materials with magnetic defects also display diffuse scattering. However, magnetic diffuse scattering is often weak, and usually obscured by the nuclear diffuse scattering, as well as thermal diffuse scattering caused by phonons and incoherent thermal excitations in the sample. Using *xyz*-NPA, one may simultaneously and unambiguously extract the nuclear and magnetic cross sections, on a multidetector spectrometer, appropriate for diffuse scattering studies of powders and single crystals.[23]

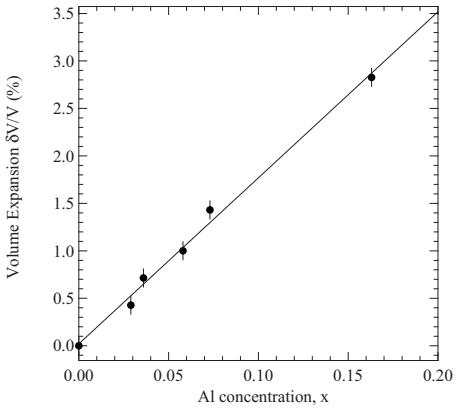


FIG. 4. Fractional volume expansion of the $\beta$-$Mn_{1-x}Al_x$ series as a function of Al concentration $x$. The straight line fit to the data indicates a rate of volume expansion of $0.17 \pm 0.01\%$ per at. % Al. in agreement with previous work (Refs. 16 and 18).

In the case of $\beta$-$Mn_{1-x}Al_x$, analysis of the nuclear diffuse neutron-scattering cross sections will tell us whether the Al substituents form a random solid solution with the Mn atoms on the $\beta$-Mn lattice, or whether they show a tendency to cluster together, or indeed, to *anticluster*, i.e., to separate themselves. The magnetic diffuse scattering will allow us to examine the Mn-Mn spin correlations of the $\beta$-$Mn_{1-x}Al_x$ alloys, and therefore to determine the extent of any short-range magnetic order in the spin-liquid (dilute Al) and spin-glass (concentrated Al) phases. Since the substituent Al atoms do not possess a magnetic moment it is clear that if there is any clustering or anticlustering of the Al substituent atoms, that will influence the nature of the Mn-Mn spin correlations. In addition, the application of polarization analysis greatly facilitates the absolute normalization of the neutron cross section in barns per atom. This then allows us to calculate the total magnetic moment participating in disordered as well as ordered magnetic phases.

The nuclear and magnetic diffuse scattering were measured using the polarization analysis neutron spectrometer, D7, at the Institut Laue-Langevin, Grenoble, using cold neutrons of wavelength 3.1 Å.

### A. Nuclear short-range order in $\beta$-$Mn_{1-x}Al_x$

In a randomly substituted binary alloy with a concentration $x$ of Al atoms having a scattering length of $b_{Al}$, and a concentration $(1-x)$ of Mn atoms with a scattering length of $b_{Mn}$, the incoherent scattering cross section (excluding nuclear spin-incoherent scattering—which is separable using *xyz*-NPA) is given by[24]

$$\left(\frac{d\sigma}{d\Omega}\right)_{inc} = \overline{b^2} - (\overline{b})^2 = xb_{Al}^2 + (1-x)b_{Mn}^2 - [xb_{Al} + (1-x)b_{Mn}]^2 = x(1-x)(b_{Al} - b_{Mn})^2. \quad (3)$$

This is termed the *Laue monotonic scattering* cross section of a binary atomic system, which will become large for a system with a large scattering length contrast $(b_{Al} - b_{Mn})$ (i.e., a large deviation of each of the individual scattering lengths from the mean). In this case, since $b_{Al}$ and $b_{Mn}$ are almost equal and opposite in sign the Laue monotonic scattering level is large. A table of the expected Laue monotonic scattering cross sections for the $\beta$-$Mn_{1-x}Al_x$ concentrations under investigation here is shown in Table II.

If the distribution of Al and Mn atoms is nonrandom, then the short-range correlations between the Al and Mn atoms will lead to a level of coherence in the diffuse scattering cross section. If we restrict our attention to the average scattering length over the ensemble of individual near-neighbor shells of atoms around a central Mn atom, the diffuse scattering in this case will be given by[24]

TABLE II. The expected Laue monotonic scattering cross sections in barns ($10^{-24}$ cm$^2$) expected for the $\beta$-$Mn_{1-x}Al_x$ concentrations in this study calculated using Eq. (3), where $x_{nom}$, $x_{calc}$ and $x_{II}$ are the nominal, calculated and site II Al concentrations, respectively.

| $x_{nom}$ | $x_{calc}$ | $x_{II}$ | $\frac{d\sigma}{d\Omega}$ calc Laue |
|---|---|---|---|
| 0.03 | 0.029 | 0.05 | 0.025 |
| 0.06 | 0.036 | 0.06 | 0.032 |
| 0.1 | 0.073 | 0.12 | 0.054 |
| 0.2 | 0.163 | 0.27 | 0.101 |

$$\left(\frac{d\sigma}{d\Omega}\right)_{\text{diff}} = \sum_{n=0}^{\infty} (\overline{b_i b_j})_n Z_n \exp(i\vec{Q}\cdot\vec{R}_n) - (\bar{b})^2$$

$$= x(1-x)(b_{\text{Al}} - b_{\text{Mn}})^2 \sum_{n=0}^{\infty} Z_n \left(1 - \frac{p_{\text{Al}}(n)}{x}\right) \times \exp(i\vec{Q}\cdot\vec{R}_n), \quad (4)$$

where $Z_n$ is the number of atoms and $p_{\text{Al}}(n)$ is the probability of finding an Al atom in the $n^{\text{th}}$ near-neighbor shell around a central Mn atom. This equation was derived separately by Cowley[25] and Warren.[26] The term in brackets, which is the Fourier coefficient of the $n^{\text{th}}$ near-neighbor shell term in the Fourier sum, is termed the *Warren-Cowley* short-range order parameter.

$$\alpha_n = 1 - \frac{p_{\text{Al}}(n)}{x} \quad (5)$$

Warren-Cowley (WC) parameters have the following properties: For the zeroth near-neighbor shell, the probability $p_{\text{Al}}(0)=0$ and therefore, $\alpha(0)=1$. For a random alloy, the probability $p_{\text{Al}}$ (cf. of finding an Al atom around a Mn atom) is equal to the concentration of Al atoms, $x$. Therefore, $\alpha(n>0)=0$, and Eq. (4) reduces to the expression for the Laue monotonic scattering [Eq. (3)]. The limiting values of the Warren-Cowley parameters are $\alpha_{\text{max}}=1$; representing a central Mn atom entirely surrounded by alike Mn atoms and $\alpha_{\text{min}}=1-\frac{1}{x}$; for a central Mn atom entirely surrounded by unlike Al atoms. For the analysis of the polycrystalline samples used in this study, we take the orientational average over all directions of the position vector $\vec{R}_n$, and the expression for the nuclear diffuse scattering becomes

$$\left(\frac{d\sigma}{d\Omega}\right)_{\text{diff}} = x(1-x)(b_{\text{Mn}} - b_{\text{Al}})^2 \left[1 + \sum_{n=1}^{\infty} Z_n \alpha_n \frac{\sin QR_n}{QR_n}\right]. \quad (6)$$

The nuclear diffuse scattering cross sections of $\beta$-$Mn_{1-x}Al_x$ with $x=0.03$, 0.04, 0.07 and 0.16 are shown in Fig. 5. Ordinarily, it should be possible to fit the nuclear diffuse scattering to Eq. (6) using least-squares refinement by varying the first $n$-neighbor WC parameters (with a judicious choice of $n$). However, in the case of the noncentrosymmetric $\beta$-Mn lattice, the number of near-neighbor shells required to model the diffuse peak would be somewhat high. To illustrate this point, the spectra shown in Fig. 5 all exhibit a peak at around $Q=1.7$ Å, with a width of ~0.8 Å. This indicates a length scale for the short-range correlations of $\sim\frac{2\pi}{0.8}=7.8$ Å. In the $\beta$-Mn structure this distance coincides with the 25th nearest-neighbor shell—indicating that at least this number of WC parameters would be necessary to describe the data. Furthermore, the WC parameters are not independent of one another and so should ideally not be freely variable in a least-squares procedure. We have therefore chosen to model our diffuse nuclear scattering using a reverse–Monte Carlo (RMC) algorithm, such as is commonly used in the analysis of diffuse scattering (see for example Ref. 27).

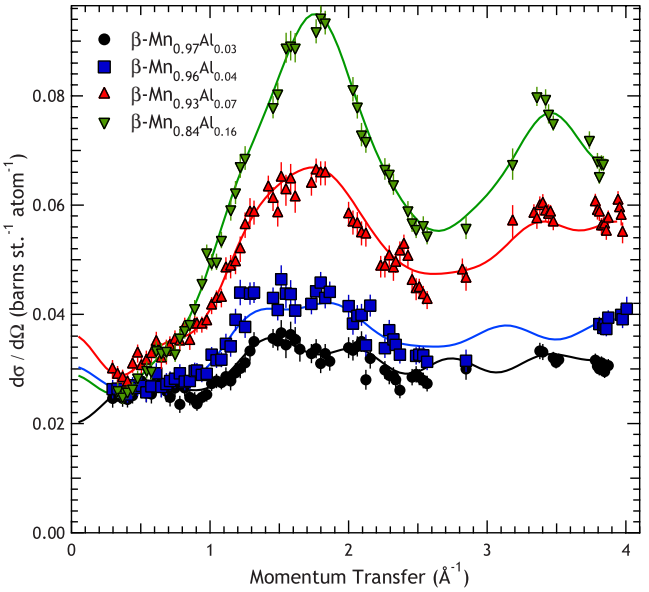


FIG. 5. (Color online) The nuclear diffuse scattering cross sections of $\beta$-$Mn_{1-x}Al_x$ with the Al concentrations shown measured at 1.5 K. The nuclear Bragg peaks have been removed from the data. The solid lines are fits to the diffuse scattering using our RMC fitting procedure (described below).

In the case of $\beta$-$Mn_{1-x}Al_x$ we assume that all the nuclear disorder scattering is due to the binary disorder model given by Eq. (6)—and hence the atomic positions are fixed, with only the Al/Mn occupations being varied. A box of $6\times6\times6$ unit cell is generated—using the site II Mn sublattice only (since Al substitutes predominantly on the site II sublattice). Al atoms are then randomly distributed on the lattice, and the corresponding differential neutron cross section is calculated according to Eq. (6). This cross section is then compared with the data and a $\chi^2$ is computed. Al atoms are then swapped with Mn atoms (one at a time) and $\chi^2$ is recomputed following each move. Moves which reduce $\chi^2$ or which increase $\chi^2$ within a Boltzmann factor defined by a temperature range chosen by the operator are accepted; other moves are rejected by the program. Figure 6 shows a typical example of the variation of the $\chi^2$ parameter as a function of RMC moves.

The solid lines in Fig. 5 show the RMC fits of Eq. (6) to the data. The WC parameters extracted from the RMC model are shown in Fig. 7. The WC parameters for all the samples studied oscillate between negative and positive values with

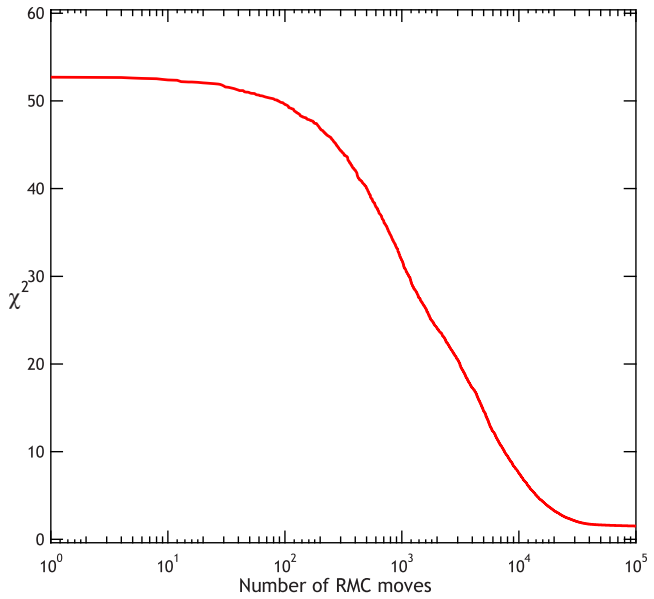


FIG. 6. (Color online) A typical example of the evolution of the $\chi^2$ goodness of fit parameter as a function of the number of RMC moves.

the first two near-neighbor WC parameters being negative. As explained above, this indicates that the chances of finding an Al atom in the first two near-neighbor shells around a central Mn atom are better than average, and that conversely, the Al atoms would rather surround a Mn atom than another Al atom. This behavior is termed *anticlustering* describing the propensity of the Al atoms to sit far apart from one another. The degree of anticlustering is seen to increase as the Al concentration increases, as indicated by the amplitude of the WC parameters in the first two shells. However, the oscillation period of the WC parameters remains broadly the same from low to high Al content. Table III gives the extracted Laue monotonic cross sections, the Al-Al anticlustering wave vector, $k_{\mathrm{Al}}$ and the Al correlation range $L_{\mathrm{Al}}$. While $k_{\mathrm{Al}}$ does not change through the series, the range of the anticlustering correlations, $L_{\mathrm{Al}}$, increases from $\sim$1 Å $-$2 Å as the Al concentration increases. The measured Laue monotonic scattering cross sections are seen to be very close to the expected values (based solely on the measured Al concentration from Sec. III), with the exception of the $x$=0.16 alloy. The measured Laue cross section of 0.069 barns for this sample implies an Al concentration of $x$=0.08—clearly at odds with the value of the lattice constant and Al concentration measured directly using neutron powder diffraction in Sec. III. The reason for this discrepancy is unclear, but it may be due to systematic errors in the data-reduction procedure—such as absorption corrections. In any case, we continue to assume that the concentration of this sample is $x$=0.16 as measured using the conventional diffraction data.

The fact that the Al impurities preferentially surround Mn atoms (as opposed to other Al atoms) would be expected to have a major effect on the magnetic properties of $\beta$-$Mn_{1-x}Al_x$. Assuming the "perfect" $\beta$-Mn structure, then each site II Mn atom has six site II near neighbors. Taking as an example the $x$=0.16 alloy, the first near-neighbor WC

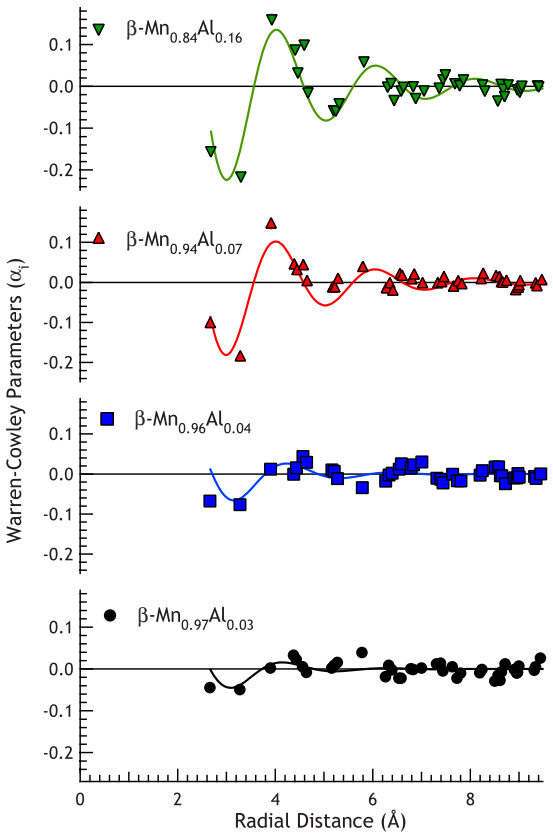


FIG. 7. (Color online) The extracted Warren-Cowley parameters from the RMC fits of the nuclear diffuse scattering from the $\beta$-$Mn_{1-x}Al_x$ alloys shown as a function of radial shell distance from a central Mn atom. The solid lines through the points are fits to a damped cosine function.

parameter is $-0.15$, giving a probability of $p_{\mathrm{Al}}$=0.31 of finding an Al atom in that shell. That translates roughly to two out of every six first near-neighbor atoms being Al—representing a major disruption to the local coordinations of the Mn atoms and greatly reducing the degree of frustration in the lattice. It is evident that the Al short-range order described here will greatly influence the magnetic ground-state properties of the alloys in this series.

### B. Magnetic short-range order in $\beta$-$Mn_{1-x}Al_x$

The magnetic neutron cross section from a disordered magnet such as a paramagnet or a static spin glass with one magnetic species can be written as

TABLE III. Summary of the RMC nuclear scattering models derived from the WC parameters shown in Fig. 7. The parameters: $k_{\mathrm{Al}}$—the Al anticlustering wave vector, and $L_{\mathrm{Al}}$—the Al correlation range, were derived by fitting a damped cosine function to the derived WC parameters shown in Fig. 7.

| $x_{\mathrm{calc}}$ | $\frac{d\sigma}{d\Omega}^{\mathrm{meas}}_{\mathrm{Laue}}$ (b) | $\frac{d\sigma}{d\Omega}^{\mathrm{calc}}_{\mathrm{Laue}}$ (b) | $k_{\mathrm{Al}}$ (Å$^{-1}$) | $L_{\mathrm{Al}}$ (Å) |
|---|---|---|---|---|
| 0.03 | 0.031(4) | 0.025 | 2.95(2) | 1.01(9) |
| 0.04 | 0.04(1) | 0.032 | 2.95(2) | 1.18(8) |
| 0.07 | 0.05(1) | 0.053 | 3.09(2) | 1.78(9) |
| 0.16 | 0.069(8) | 0.101 | 3.08(2) | 2.04(8) |

$$\left(\frac{d\sigma}{d\Omega}\right)_{\text{Mag}} = q^2\left(\frac{\gamma_n r_0^2}{2}\right)^2 f^2(\vec{Q})S(\vec{Q})M^2(\vec{Q}), \tag{7}$$

where $M(\vec{Q})$ is the Fourier transform of the spatially varying magnetization density $M(\vec{r})$, and $S(\vec{Q})$ is the nuclear structure factor. $\vec{q}$ is the so-called *magnetic interaction vector* $\vec{q} = \hat{Q}(\hat{Q}\cdot\hat{M}) - \hat{M}$. In the case of a randomly oriented magnet we have for the magnetic interaction vector

$$q^2 = 1 - (\hat{Q}\cdot\hat{M})^2 = \frac{2}{3}. \tag{8}$$

$M^2(\vec{Q})$ can be written as

$$M^2(\vec{Q}) = g_S^2 S(S+1)\sum_n \frac{\langle \vec{S}_0\cdot\vec{S}_n\rangle}{S(S+1)}\exp(i\vec{Q}\cdot\vec{r}_n), \tag{9}$$

where $\vec{S}_0$ and $\vec{S}_n$ are the atomic spin vectors at the origin and the $n$th nuclear lattice position. Factorizing Eq. (9) into near-neighbor shells, and taking the powder average, we arrive at the expression

$$\left(\frac{d\sigma}{d\Omega}\right)_{\text{Mag}} = \frac{2}{3}\left(\frac{\gamma_n r_0^2}{2}\right)^2 f^2(\vec{Q})g_S^2 S(S+1) \times\left[1 + \sum_n \frac{\langle \vec{S}_0\cdot\vec{S}_n\rangle}{S(S+1)} Z_n \frac{\sin Qr_n}{Qr_n}\right], \tag{10}$$

where $r_n$ and $Z_n$ are the radius and coordination number of the $n$th near-neighbor shell, and where we have assumed that $S(\vec{Q})=1$; i.e., there are no nuclear structure driven magnetic fluctuations. However, in the case of $\beta$-$Mn_{1-x}Al_x$ we know that we cannot make this assumption, and that the form of $S(\vec{Q})$ modeled in Sec. IV A should have an influence over the nature of the magnetic correlations. Therefore, in going from Eq. (7) to Eq. (10) one must perform the powder average of $M^2(\vec{Q})$ and $S(\vec{Q})$ simultaneously. In all but the simplest structures (see for example Ref. 28), this calculation is very difficult, and numerical modeling methods must be used to take full account of the nuclear and magnetic contributions to the magnetic diffuse cross section. In addition, the magnetic correlations $\langle \vec{S}_0\cdot\vec{S}_n\rangle$ are not independent parameters—but are in fact, highly correlated. This is easily seen by the fact that a strong negative first near-neighbor correlation necessarily leads to a strong positive correlation at twice this distance.

Therefore we have modeled our data using a reverse–Monte Carlo algorithm similar to that used for modeling the nuclear binary disorder scattering. The simulated nuclear model is used as input to the magnetic calculation, with magnetic moments being assigned only to the magnetic site II (12*d*) Mn atoms. In this way the nuclear disorder is automatically taken into account. Spins of magnitude $S$ are then randomly oriented on the site II Mn positions, and the diffuse cross section is calculated according to Eqs. (7) and (10). Individual spins are then randomly rotated one at a time, and this rotation is accepted or rejected on the basis of the $\chi^2$ criterion described in the previous section.

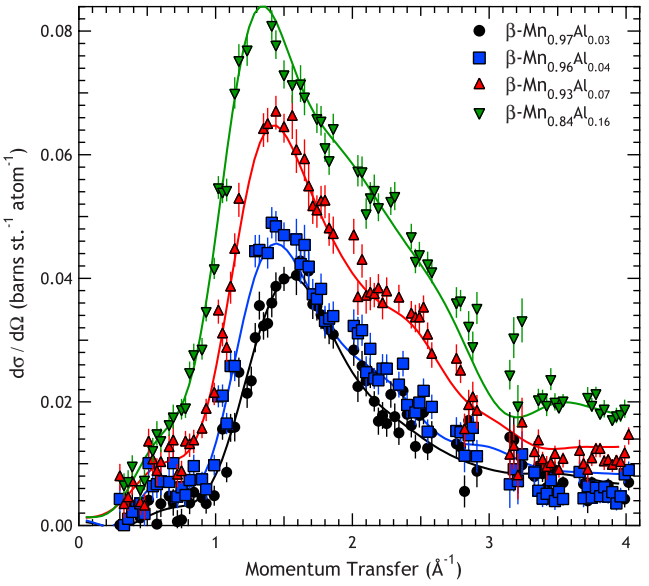


FIG. 8. (Color online) The magnetic diffuse scattering of the $\beta$-$Mn_{1-x}Al_x$ alloys shown measured at 1.5 K. The solid lines through the data are RMC fits of the data to Eqs. (7) and (10).

The magnetic diffuse scattering cross sections and the near-neighbor correlation parameters extracted from the RMC fitting procedure are shown in Figs. 8 and 9. In all the samples under investigation, the first near-neighbor correlation parameter is strongly negative—indicating predominantly antiferromagnetic correlations. Also evident from the data is that, despite that fact that the degree of topological frustration in the $\beta$-Mn lattice is being lifted by the Al impurity substituents, there is no sign of long-range magnetic order in these alloys. Indeed, an initial inspection of the correlation parameters in Fig. 9 reveals that the range of the correlations stays roughly the same across the Al concentration range studied here, with the strongest correlation amplitudes appearing at $x=0.07$. Table IV gives the spin and moment values, the antiferromagnetic correlation distance, $1/k_{\text{mag}}$ (given by the oscillation period of the magnetic correlations) and the magnetic cluster size, $L_{\text{mag}}$, the latter two parameters extracted from the magnetic correlations by fitting a damped cosine function as shown in Fig. 9.

With the exception of the $x=0.03$ sample (which only displays a strong AF correlation in the first near-neighbor shell), all the alloys studied show the same AF correlation distance at around 3.3 Å. For the $x=0.03$ sample, a correlation distance of 4.8 Å is roughly twice the Mn-Mn near-neighbor distance, while for the higher Al concentrations, 3.3 Å corresponds to the second near-neighbor shell. For $x=0.03$, 0.04 and 0.16, the range of the magnetic correlations, $L_{\text{mag}}$, is around 2 Å, whereas for the $x=0.07$ concentration it is somewhat longer at 2.6 Å. The Mn moment rises from 0.8 $\mu_B$ for $x=0.03$ to around 1.5 $\mu_B$ for $x=0.16$: roughly linear with Al concentration. The Mn moment across the series is plotted in Fig. 10.

## V. DISCUSSION

The fact that the magnetic structure factor $M^2(\vec{Q})$ and hence the short-range correlations change little throughout

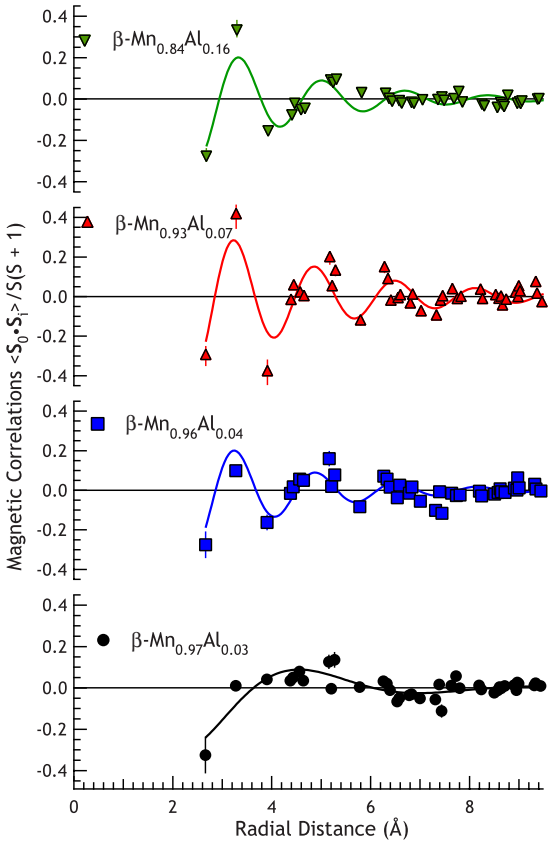


FIG. 9. (Color online) Magnetic correlation parameters for the $\beta$-$Mn_{1-x}Al_x$ shown extracted from the RMC modeling procedure as described in the text. The solid lines through the data are fits to a damped cosine function.

the series of $\beta$-$Mn_{1-x}Al_x$ samples measured in this study indicates that the transition from spin-liquid to spin-glass-like order as observed using $\mu$SR (Ref. 19) is purely dynamical in nature; i.e., there is no evidence of a magnetic structural transition across the 9 at.% critical concentration identified by $\mu$SR (see Fig. 2).

One possible picture is that, as the Al atoms are substituted onto the site II Mn sublattice—disrupting the local Mn-Mn coordination and therefore lifting the spin-configurational degeneracy—the amount of *magnetic* disorder introduced effectively inhibits the formation of a long-range ordered magnetic ground state. Evidence for this picture may be drawn from the fact that the effective magnetic cluster size (given by the range of the magnetic correlations—or equivalently—the sharpness of the peak in the magnetic structure factor) reaches a maximum value at the intermediate $x=0.07$ concentration, indicating the point of best compromise between reduction of frustration and introduction of disorder.

TABLE IV. Summary of the RMC magnetic scattering models derived from the magnetic correlations shown in Fig. 9. The parameters: $1/k_{mag}$—the magnetic correlation distance, and $L_{Al}$—the magnetic correlation range were derived by fitting a damped cosine function to the derived short-range magnetic correlations shown in Fig. 9.

| $x_{calc}$ | $S(S+1)$ | $\mu$ | $1/k_{mag}$ (Å) | $L_{mag}$ (Å) |
|---|---|---|---|---|
| 0.03 | 0.17(5) | 0.8(1) | 4.8(1) | 1.9(1) |
| 0.04 | 0.20(5) | 0.9(1) | 3.34(2) | 2.0(1) |
| 0.07 | 0.32(5) | 1.17(9) | 3.26(2) | 2.6(2) |
| 0.16 | 0.49(5) | 1.52(7) | 3.36(2) | 2.1(1) |

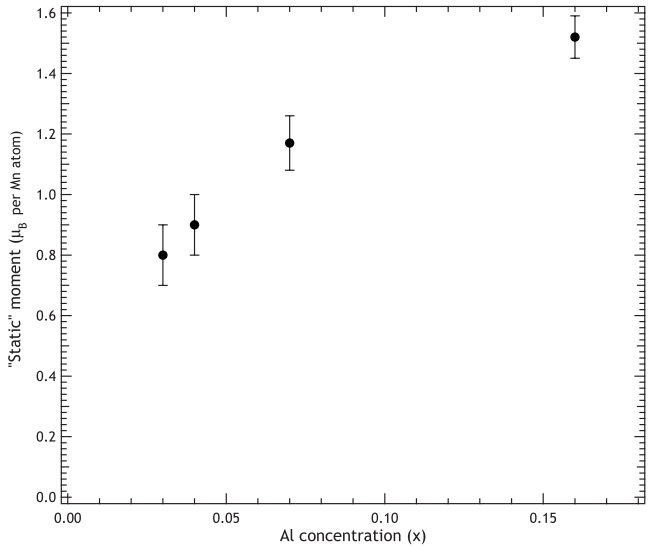


FIG. 10. The diffuse "static" magnetic moment per Mn atom in $\beta$-$Mn_{1-x}Al_x$ as a function of Al concentration $x$ and derived from the RMC fits of the magnetic diffuse scattering data as described in the text.

*xyz*-NPA has allowed us to extract the magnetic moment per Mn atom for each of the $\beta$-$Mn_{1-x}Al_x$ samples studied. The apparent increase in the magnetic moment on increasing Al concentration $x$ may indicate a real increase in the Mn magnetic moment—perhaps due to the formation of local magnetic moments concomitant with the lattice expansion (and hence the increased Mn-Mn near-neighbor distance) caused by Al doping (see Fig. 4). However, there is another possible explanation for this behavior. The incident neutron energy of 8.5 meV used for this experiment represents the upper limit of the spin-fluctuation frequencies measurable. In other words, the diffuse scattering cross sections measured will represent a sum over spin-fluctuation energies up to a maximum of 8.5 meV (the actual maximum energy measured depends on the scattering triangle formed by the incident neutron wave vector $\vec{k}_i$, the final wave vector $\vec{k}_f$, and the wave-vector transfer $\vec{Q}=\vec{k}_i-\vec{k}_f$). Therefore if there exist fluctuations in the magnetic system under investigation, then the full magnetic moment will only be measurable on a neutron spectrometer when the energy width of the fluctuations, $\hbar\Gamma \ll \hbar^2 k_i^2/k_B T$. Our $\mu$SR results on $\beta$-$Mn_{1-x}Al_x$ alloys with $x<0.09$ show that, while there is an indication of a critical slowing of the spin fluctuations at low temperatures, a fast fluctuating dynamical component remains at 1.5 K. Only in $\beta$-$Mn_{1-x}Al_x$ alloys with $x>0.9$ was there an indication of a truly "static" magnetic state on the time scale of the muon lifetime (2.2 $\mu$s).[19] Given that this is a much longer time scale than that of the cold neutron spectrometer (here $\lambda$

$=3.1$ Å $\equiv \sim 10^{-12}$ s) then it can be safely assumed that the full magnetic moment will be measured only for the $x=0.16$ sample. For the other samples it is likely that broad low-temperature spin fluctuations outside the spectrometer time-window result in an apparent reduction in the measured moment. Indeed for pure $\beta$-Mn it is well known that extremely broad (up to 40 meV) spin fluctuations exist at low temperatures[7]—and it was for this reason that a measurement of the $\beta$-$Mn_{1-x}Al_x$ with $x=0$ was not attempted in this investigation.

It should be noted that our analysis of the diffuse scattering data presented in this study is based on a model of magnetic moments existing on only the site II ($12d$) lattice positions—as indicated by NMR studies.[5] The diffuse scattering data unfortunately do not provide any *a priori* evidence for a lack of magnetic moment on the site I Mn sites. This is due to the fact that the local coordinations and near-neighbor distances of sites I and II are very similar, each of which is capable of giving rise to the observed magnetic diffuse scattering cross sections.

## VI. CONCLUSIONS

In conclusion, we have carried out a survey of low-temperature magnetic short-range order in $\beta$-$Mn_{1-x}Al_x$ alloys using a reverse–Monte Carlo procedure which first models the nuclear disordered structure of the solid solution of Al in Mn, and then uses this nuclear structure as the basis of a calculation of the disordered magnetic structure factor. We have measured the nuclear and magnetic structure factors using *xyz*-neutron polarization analysis which allows the unambiguous determination of the nuclear and magnetic contributions to the neutron-scattering cross sections. In this way we have extracted the Mn-Mn spin correlations at low temperatures for $\beta$-$Mn_{1-x}Al_x$ alloys with $x=0.03$, 0.04, 0.07 and 0.16. We see no evidence of any significant evolution of the magnetic structure, or increase in the magnetic correlation lengths in these alloys as the spin-liquid to spin-glass transition is crossed (at $x=0.09$). We suggest that this may be due to a trade-off between strong geometrical frustration in the dilute $\beta$-$Mn_{1-x}Al_x$ alloys, giving way to significant magnetic local disorder for the more concentrated alloys.

## ACKNOWLEDGMENTS

The authors would like to thank their colleagues, B. D. Rainford, A. P. Murani, D. A. Keen and S. H. Kilcoyne, for their experimental assistance and very useful discussions. We would also like to thank the instrumental support staff both at the ILL, Grenoble and ISIS for their assistance in the smooth running of the neutron-scattering experiments. Financial support from the UK Engineering and Physical Sciences Research Council is gratefully acknowledged.

*R.stewart@rl.ac.uk

[1] T. Moriya, *Spin Fluctuations in Itinerant Electron Magnetism* (Spinger-Verlag, Berlin, 1985).
[2] M. J. P. Gingras, C. V. Stager, N. P. Raju, B. D. Gaulin, and J. E. Greedan, Phys. Rev. Lett. **78**, 947 (1997).
[3] C. B. Shoemaker, D. P. Shoemaker, T. E. Hopkins, and S. Yindepit, Acta Crystallogr., Sect. B: Struct. Crystallogr. Cryst. Chem. **34**, 3573 (1978).
[4] P. I. Kripyakevich, Sov. Phys. Crystallogr. **5**, 253 (1960).
[5] Y. Kohori, Y. Noguchi, and T. Kohara, J. Phys. Soc. Jpn. **62**, 447 (1993).
[6] T. Shinkoda, K. Kumagai, and K. Asayama, J. Phys. Soc. Jpn. **46**, 1754 (1979).
[7] J. R. Stewart, B. D. Rainford, R. S. Eccleston, and R. Cywinski, Phys. Rev. Lett. **89**, 186403 (2002).
[8] N. Bernhoeft, J. Phys.: Condens. Matter **13**, R771 (2001).
[9] T. Kohara and A. Asayama, J. Phys. Soc. Jpn. **37**, 401 (1974).
[10] M. Shiga, H. Nakamura, M. Nishi, and K. Kakurai, J. Phys. Soc. Jpn. **63**, 1656 (1994).
[11] S. Funahashi and T. Kohara, J. Appl. Phys. **55**, 2048 (1984).
[12] Y. Nakai, J. Phys. Soc. Jpn. **63**, 775 (1994).
[13] K. Sasao, R. Y. Umetsu, and K. Fukamichi, J. Alloys Compd. **325**, 24 (2001).
[14] M. Miyakawa, R. Y. Umetsu, M. Ohta, A. Fujita, K. Fukamichi, and T. Hori, Phys. Rev. B **72**, 054420 (2005).
[15] J. R. Stewart, A. S. Wills, C. J. Leavey, B. D. Rainford, and C. Ritter, J. Phys.: Condens. Matter **19**, 145291 (2007).
[16] H. Nakamura, K. Yoshimoto, M. Shiga, M. Nishi, and K. Kakurai, J. Phys.: Condens. Matter **9**, 4701 (1997).
[17] B. Canals and C. Lacroix, Phys. Rev. B **61**, 11251 (2000).
[18] J. R. Stewart, Ph.D. thesis, University of St. Andrews, 1998.
[19] J. R. Stewart and R. Cywinski, Phys. Rev. B **59**, 4305 (1999).
[20] I. A. Campbell, A. Amato, F. N. Gygax, D. Herlach, A. Schenck, R. Cywinski, and S. H. Kilcoyne, Phys. Rev. Lett. **72**, 1291 (1994).
[21] A. C. Larson and R. B. V. Dreele, Los Alamos National Laboratory Technical Report No. LAUR-86-748, 1994.
[22] O. Schärpf and H. Capellmann, Phys. Status Solidi A **135**, 359 (1993).
[23] J. R. Stewart, K. H. Andersen, R. Cywinski, and A. P. Murani, J. Appl. Phys. **87**, 5425 (2000).
[24] G. L. Squires, *Introduction to Thermal Neutron Scattering* (Cambridge University Press, Cambridge, 1978).
[25] J. M. Cowley, Phys. Rev. **77**, 669 (1950).
[26] B. E. Warren, B. L. Averbach, and B. W. Roberts, J. Appl. Phys. **22**, 1493 (1951).
[27] A. Mellergård, R. L. McGreevy, A. Wannberg, and B. Trostell, J. Phys.: Condens. Matter **10**, 9401 (1998).
[28] R. Cywinski and T. J. Hicks, J. Phys. F: Met. Phys. **10**, 693 (1980).